Journal of Superconductivity and Novel Magnetism (2021) 34:3151–3161
https://doi.org/10.1007/s10948-021-06072-w

ORIGINAL PAPER

Comparing of the Magnetic Force Parameters of Superconducting Maglev System Using Horizontal and Vertical PMG Geometry in Multi-Surface HTS-PMG Arrangement

Kemal Ozturk[1] · Burcu Savaskan[2] · Murat Abdioglu[1,3] · Ahmet Cansiz[4] · Durukan Burak Dilek[5] · Zekeriya Karaahmet[6]

Received: 23 August 2021 / Accepted: 4 October 2021 / Published online: 6 November 2021
© The Author(s), under exclusive licence to Springer Science+Business Media, LLC, part of Springer Nature 2021

Abstract
In this study, a detailed static and dynamic experimental studies were carried out in different cooling heights (CH) by using two different multi-surface HTS-PMG arrangements with horizontal (MS-H) and vertical (MS-V) geometries to determine the optimum magnetic force, static stiffness, dynamic response, and dynamic stiffness parameters of superconducting Maglev system. The maximum levitation force values (in CH = 25 mm) were obtained as 202 N and 84 N, respectively, with horizontal and vertical geometry HTS-PMG arrangements, while the maximum guidance force values (in CH = 5 mm) were obtained as −58 N and −22 N, respectively. Also, the vertical static (in CH = 25 mm) and dynamic stiffness (in CH = 5 mm) values were determined as 33.8 N/mm and 37.8 N/mm, respectively, for MS-H and 12.3 N/mm and 25.1 N/mm, respectively, for MS-V arrangements. The bigger levitation force, guidance force, and both static and dynamic magnetic stiffness values of MS-H arrangement with horizontal geometry than that of MS-V arrangement with vertical geometry indicate that the horizontal HTS-PMG geometry is more suitable for practical Maglev applications in terms of loading capacity and movement stability.

Keywords Multi-surface · HTS Maglev · Magnetic parameters · Magnetic flux profile · Levitation force

1 Introduction

High-temperature superconductors (HTS) can trap larger magnetic fields than conventional permanent magnets (PM) and also provide stable levitation and suspension [1–5]. Due to their unique properties as magnetic suspension and almost zero resistivity, HTS bulks can be utilised for the development of superconducting magnetic bearings [6, 7], motors/generators [8], and superconducting magnetic levitation (SML) transportation system (Maglev) [9, 10]. At the present time, Maglev trains are renowned innovative technologies because they use non-contact movement above a magnetic rail (permanent magnetic guideway: PMG) and also have no wheels, axles, and transmission. Moreover, compared to traditional high-speed railroad vehicles, Maglev is more environmentally friendly due to its low-energy consumption, lower noise, and higher speed of travel [11–13]. Up to now several superconducting Maglev vehicle prototypes have been successfully developed. The first demonstration of a SML vehicle with man-loaded was made at Southwest Jiaotong University in China; in 2002, later some Maglev prototypes were developed in Brazil and Germany [10, 14, 15].

The electromagnetic force between a permanent magnet and a superconductor makes the system stable as different from the PM, because the magnetic flux lines are pinned in the HTS and this situation causes vertical suspension and lateral guidance forces. In the Maglev system,

✉ Kemal Ozturk
kozturk@ktu.edu.tr

[1] Department of Physics, Faculty of Science, Karadeniz Technical University, Trabzon 61080, Turkey

[2] Department of Energy Systems Engineering, Faculty of Technology, Karadeniz Technical University, Trabzon 61800, Turkey

[3] Department of Mathematics and Science Education, Faculty of Education, Bayburt University, Bayburt 69000, Turkey

[4] Electrical Engineering Department, Faculty of Electrical and Electronics, Istanbul Technical University, Istanbul 34469, Turkey

[5] Department of Mechanical Engineering, Faculty of Engineering, Karadeniz Technical University, Trabzon 61080, Turkey

[6] Department of Renewable Energy Sources Technologies, Graduate School of Science, Karadeniz Technical University, Trabzon 61080, Turkey

the levitation force is able to levitate the train to eliminate mechanical friction, while the guidance force keeps the train on moving along the permanent magnetic rail. Superconducting Maglev vehicles do not need complex control systems due to the Meissner and pinning effects of the HTS bulks. SML trains arise from a superconducting part which carrying the vehicle or load and a PMG magnetic rail providing the magnetic force at a large distance. Although SML trains are well suited to urban transportation, the disadvantage of these systems is high cost of permanent magnets that should paved along long distances as thousands of kilometres. It was shown in a study on cost analysis that, if a PM (N42) would remove from each unit arrays, 25×10^6 fewer PMs are needed for 1000 km length, and this case causes approximately € 750 million saving without a significant decrement in levitation force [16]. Several research groups have done some experimental and theoretical studies to improve the levitation and guidance forces by using different HTS-PMG arrangements [17–22]. In addition, the optimum design and physics of PMG configurations [23], such as the pole numbers [24, 25] and the effect of the size and shape of both PM and HTS [26, 27], have been studied in a number of papers. Also, our research group has done some studies and progress to determine optimum parameters of Maglev system such as the cooling height (CH), the pole arrays of the PMG, and the arrangements of PMG-HTS [24, 25, 28]. It was reported in above studies that the loading capacity and movement stability of single surface Maglev systems can be enhanced via suitable CH, pole number, and HTS-PMG arrangements. Although some enhancements have been achieved on loading capacity and stability of Maglev systems in above studies, additional studies are necessary in terms of lower fabrication cost and higher efficiency of Maglev systems for technological applicability of these systems. The studies in literature have focused on improving the loading capacity via increasing the PM and/or HTS number in the single surface (that is the HTS and PMG units are interacted along only one axes) Maglev system. Basaran et al. [29] have obtained an increment in the magnetic levitation force (44.25%) using multi-surface levitation concept with three ring PMs and one HTS ring for flywheel superconducting bearing system by increasing PM number. However, the force density in unit volume of Maglev systems can be increased by increasing the interaction surface number of HTS and PMG rather than increasing the PM number. Therefore, for increasing both the loading capacity and movement stability, the multi-surface HTS-PMG arrangements (that is, the HTS and PMG units are interacted along two axes) are investigated in this study by using horizontal and vertical PMG geometry. The multi-surface arrangements give us the possibility to increase the HTS number in unit volume to compensate the magnetic force due to decreased PM number paved along in thousands of kilometres PMG. In the present study, firstly, the magnetic flux density distributions of the horizontal and vertical PMGs were determined via numerical method using the finite element method. Then, a detailed static and dynamic experimental studies were performed in different cooling heights by using two different multi-surface HTS-PMG arrangements to determine the optimum magnetic force, static stiffness, dynamic response, and dynamic stiffness parameters of superconducting Maglev system.

2 Experimental and Numerical Procedure

The magnetic field distributions of the PMGs were determined by numerical modelling (in two dimensions) via magnetostatic solution in COMSOL Multiphysics 3.5 by taking the magnetization value of each PM as 1132490 A/m, and the details can be found in [16].

The static and dynamic force measurements were carried out via the three axes magnetic levitation force measurement system (TAMFS) [16, 24]. Three-seeded rectangular prism shaped YBaCuO superconductors with dimensions of 65 mm × 34 mm × 14 mm were provided by ATZ GmbH, Germany. The dimensions and surface magnetic flux densities of PMs used in PMGs are 40 mm × 30 mm × 30 mm and 0.53 T, respectively. The horizontal and vertical PMG geometries are used in this study as schematically seen in Fig. 1. The abbreviations of (MS-H) and (MS-V) in Fig. 1, respectively, represent horizontal and vertical PMG geometries in multi-surface HTS-PMG arrangements. An iron block of 10 mm width, as seen in Fig. 1, is placed between the PMs in MS-V arrangement in vertical geometry to overcome the physical challenge to bring two oppositely directed PMs together. The HTS sample chambers are handmade from 6013 series aluminium material, and the PMGs are fixed to the measurement system via aluminium support legs.

We have measured the vertical magnetic levitation force in different cooling heights (CHs: the vertical distance between the upper surface of the PMG and bottom surface of the upper HTSs) of 5 mm and 25 mm and the lateral guidance force measurements in CH of 5 mm and working height (WH) of 10 mm. We have calculated the vertical magnetic stiffness values from the levitation force measurements in CH = 25 mm by making minor cycles on levitation force curves to obtain minor loops at different vertical positions of $z = 5$, 9, 13, and 17 mm. For the minor cycle at the position of $z = 17$ mm, the stiffness calculation is performed as follows: After completely cooling of the HTSs, the vertical distance between the PMG and HTS units is decreased from 75 to 17 mm, then increased to 19 mm ($\Delta z = 2$ mm), and

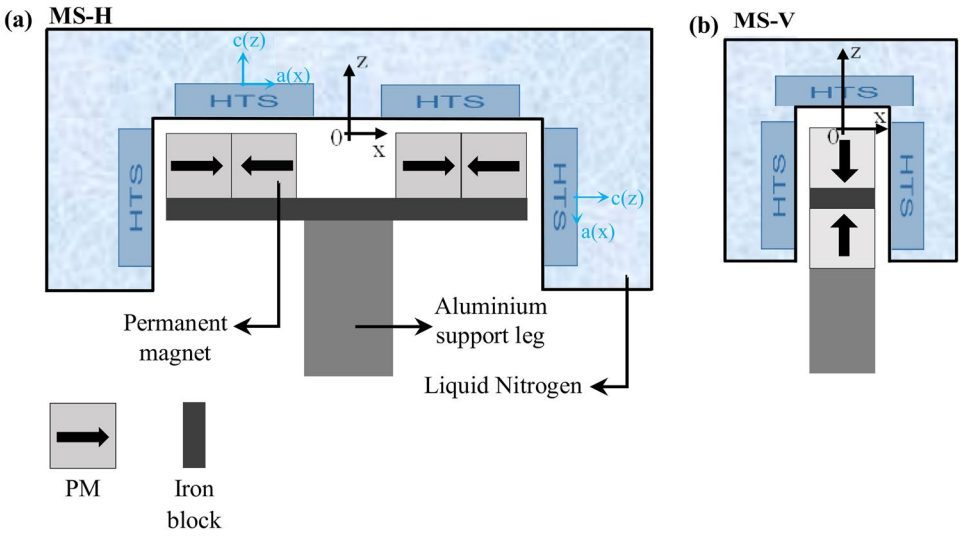


Fig. 1 Schematic view of MS-H (**a**) and MS-V (**b**) multi-surface HTS-PMG arrangements (the arrows on the PMs represent the magnetic pole direction)

finally decreased to 13 mm for the next minor cycle. Then, these cycles are fitted with a linear line, and the product of the slopes of these linear lines by negative gives us the related magnetic stiffness values. The same procedure is performed at the positions of $z = 13$ mm, 9 mm, and 5 mm for calculating the related magnetic stiffness values. We have also calculated the lateral magnetic stiffness values similar to the vertical magnetic stiffness by making minor loops at different lateral positions of $x = 1$, 2, and 3 mm, and detailed information about all measurement procedures can be found in our previous studies [24, 28].

The resonance frequency and dynamic stiffness parameters of MS-H and MS-V multi-surface HTS-PMG arrangements were determined via dynamic force measurement system integrated to TAMFS. The dynamic measurements were performed in different CHs of 5 mm, 7 mm, and 10 mm. The vertical dynamic response characteristics of MS-H and MS-V arrangements were determined by applying an impulse force via a hammer (PCB model-086C03) to r top centres of the chambers (with total mass of 4.48 kg and 3.45 kg, respectively) to trigger an oscillation, and then releasing the HTS sample chamber to levitate freely above the related PMGs. The free vibration data were collected via NI-9234 4-Channel 24-Bit vibration input module equipped with B&K triaxial accelerometer (model 4524-B), and the vibration signals were analysed via a script developed in MATLAB. This script is written by using transform function library to able to calculate frequency response function accurately. To obtain the vibration behaviour of the multi-surface HTS-PMG system, fast Fourier transformation (FFT) was applied to the acceleration and force data obtained by data acquisition system. The sampling time was 2 s with sampling time interval of 0.5 ms and frequency band 0–100 Hz in dynamic response measurements.

3 Results and Discussion

Since the HTSs are located both at the top and side surfaces of the PMGs, the magnetic flux profiles should be determined in each sides. The vertical (B_z) and lateral (B_x) magnetic flux density distributions of MS-H and MS-V multi-surface HTS-PMG arrangements obtained from 5 mm above the top surface of the PMGs are shown in Fig. 2. To avoid any complicity in thereafter physical interpretation in the text, the *c*- and *a*-axes (in blue colour) in Fig. 1, respectively, represent the crystal growth axis and perpendicular to *c*-axis of the HTS that is fabricated by top seeded melt growth method. The inset figures in Fig. 2 show the magnetic flux density distributions at 5 mm obtained from the right surfaces of the PMGs. Maximum vertical magnetic flux density (B_z) values at 5 mm from top surfaces are obtained as 0.69 T and 0.48 T, respectively, for MS-H and MS-V arrangements, while these values are obtained, respectively, as 0.44 T and 0.58 T at 5 mm from the right surfaces. In addition, the maximum lateral magnetic flux density (B_x) values at 5 mm from top surfaces are obtained as 0.40 T and 0.38 T, respectively, for MS-H and MS-V arrangements, while these values are obtained, respectively, as 0.11 T and 0.39 T at 5 mm from the right surfaces.

Figure 3 shows the magnetic levitation force comparison of multi-surface MS-H and MS-V arrangements in CH = 25 mm and CH = 5 mm. The maximum levitation force values are obtained as 202 N and 84 N, respectively, for MS-H and MS-V arrangements in CH = 25 mm. On the other hand, in CH = 5 mm, the maximum levitation force values are obtained as 37 N and 18 N in addition to attractive force values of −82 N and −34 N, respectively, for MS-H and MS-V arrangements, as can be seen in Fig. 3b. The magnetic levitation force, F_z, can be defined as Eq. (1), where J_y

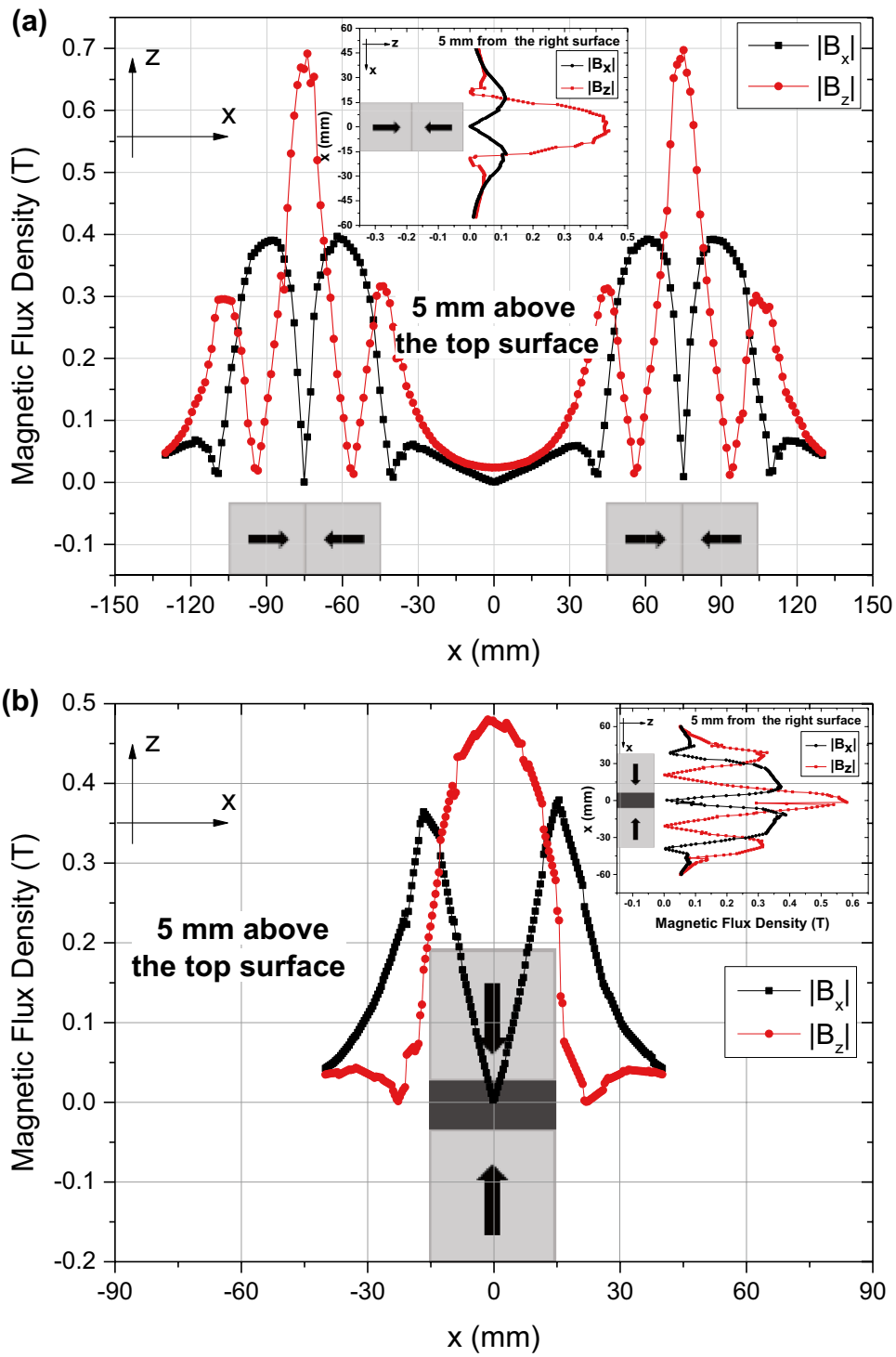


Fig. 2 Magnetic flux density distributions of MS-H (**a**) and MS-V (**b**) multi-surface HTS-PMG arrangements obtained at a distance of 5 mm from the top surfaces of the PMGs. Inset figures show the magnetic flux density distributions 5 mm from the right surfaces of PMGs

(circulating in ab plane of the HTSs) represents the induce supercurrent inside the HTS in *y*-direction and B_x represents the lateral component of magnetic flux density as can be seen in Fig. 2.

$$F_z = \int_V J_y B_x dV \tag{1}$$

One can see from Fig. 2 that both the B_z and B_x values of MS-H arrangement at the top surface of the PMG are bigger than that of MS-V arrangement. The induced supercurrent, J_y, is activated by the vertical component of the magnetic flux density (B_z), and bigger B_z values increase the J_y. On the other hand, as can be seen in Eq. (1), the levitation force

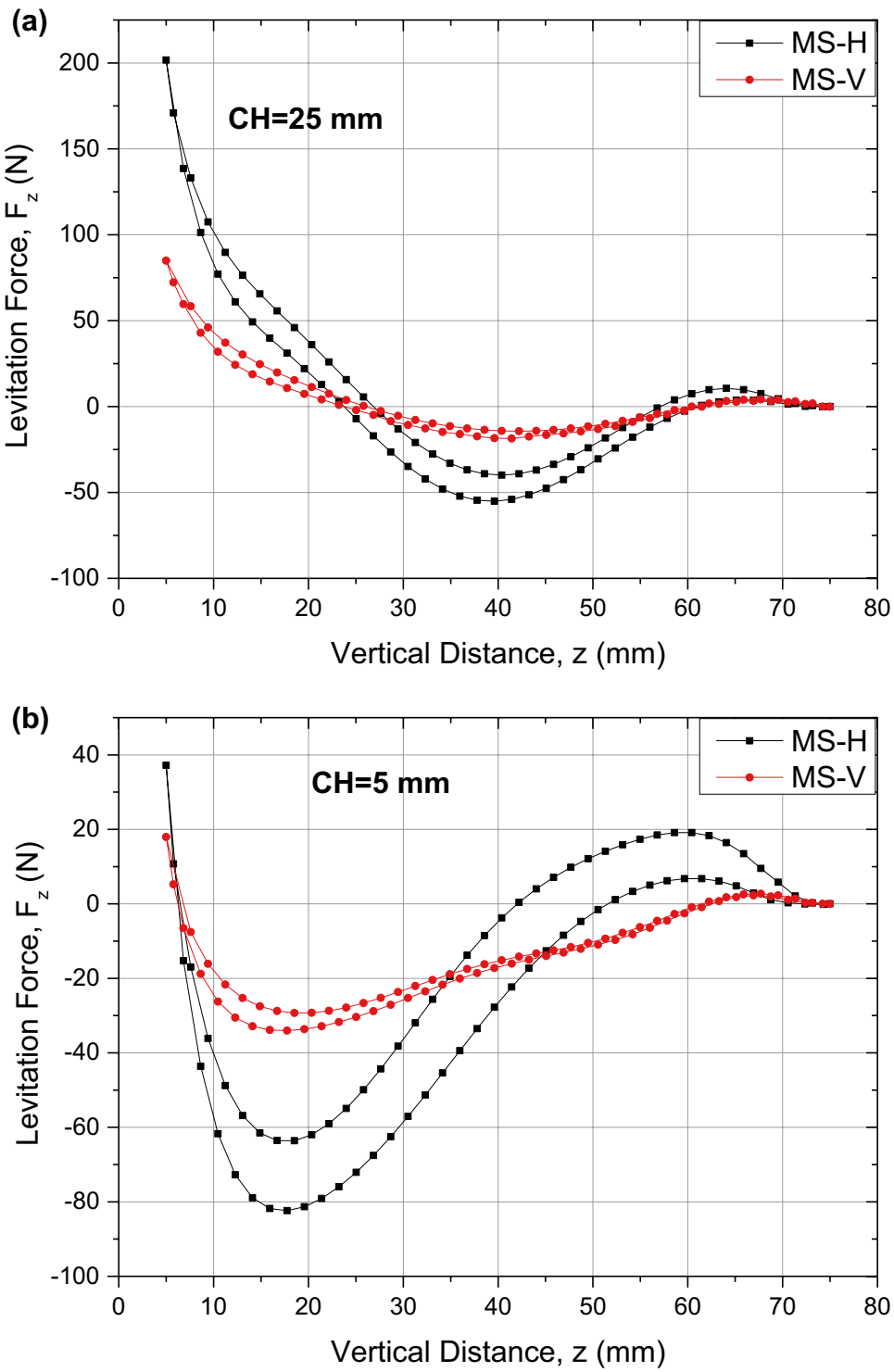


Fig. 3 Magnetic levitation force comparison of multi-surface MS-H and MS-V arrangements in CH = 25 mm (**a**) and CH = 5 mm (**b**)

depends on B_x, and therefore, bigger B_x and B_z values of MS-H arrangement produce bigger levitation force values, as shown in Fig. 3. Bigger repulsive and attractive force values of MS-H arrangements in CH = 25 mm indicate stable equilibrium of HTS-Maglev system in this cooling height, and this situation provides a movement stability in vertical direction. The maximum attractive force value of MS-H arrangement as −82 N in CH = 5 mm (Fig. 3b) indicates the trapped magnetic flux inside the HTSs in this cooling height. The bigger trapped flux and so the bigger attractive force of MS-H arrangement show that the main contribution to the trapped flux comes from the upper HTSs in the sample chamber of horizontal geometry. One can see in Fig. 1 that the MS-H arrangement has 4 PM, while MS-V arrangement

has 2 PM, and thus, it can be said that even if the levitation force is calculated for 2 PM instead of 4 PM in horizontal geometry, the MS-H arrangement is seen as superior to the MS-V arrangement in vertical geometry.

Lateral guidance force comparison of multi-surface MS-H and MS-V arrangements is shown in Fig. 4 in CH = 5 mm and for WH = 10 mm. The maximum guidance force values are obtained as −58 N and −22 N, respectively, for MS-H and MS-V arrangements. Lateral guidance force can be defined as Eq. (2), where B_z represents the vertical component of magnetic flux density as can be seen in Fig. 2.

$$F_x = \int_V J_y B_z dV \tag{2}$$

According to the above equation, as similar to the vertical levitation force, the guidance force depends on the J_y, induced supercurrent circulating inside the HTSs in ab-plane (and so the magnetic field component, perpendicular to the sample surface), and vertical component of magnetic flux density, B_z. Thus, nearly three times bigger maximum guidance force value of MS-H arrangement than that of MS-V can be attributed to bigger B_z value of MS-H arrangement. In addition, it can be said by comparing Figs. 3 and 4 that the difference between the maximum values in guidance force of MS-H and MS-V arrangements is bigger than that in levitation force values. This situation indicates that the contribution of horizontal geometry to the guidance force is bigger than that of vertical geometry.

Figure 5 shows the vertical magnetic stiffness curves of multi-surface MS-H and MS-V arrangements depending on vertical distances in CH = 25 mm. One can see from this figure that the vertical magnetic stiffness values increase with decreasing vertical distance due to increasing vertical slope of levitation force in smaller gaps as seen in Fig. 3. The bigger maximum vertical stiffness value of MS-H arrangement as 33.8 N/mm than that of MS-V arrangement as 12.3 N/mm indicates that the MS-H arrangement is more suitable for higher loadings and more resistant to external disturbances.

Lateral magnetic stiffness of multi-surface MS-H and MS-V arrangements is shown in Fig. 6 in CH = 5 mm and WH = 10 mm. It can be seen that the lateral magnetic stiffness values increase slightly with increasing lateral distance. Maximum lateral stiffness values were obtained as 16.4 N/mm and 6.2 N/mm, respectively, for MS-H and MS-V arrangements. One can see by comparing Figs. 5 and 6 that the increment rate in vertical stiffness is bigger than that in lateral stiffness values due to lower vertical and lateral magnetic flux density at the top and sides of the MS-V arrangement as shown in Fig. 2b.

In addition to the static parameters such as levitation force, guidance force, and magnetic stiffness, the dynamic vibration parameters were also investigated in this study to determine the dynamic behaviour of Maglev systems

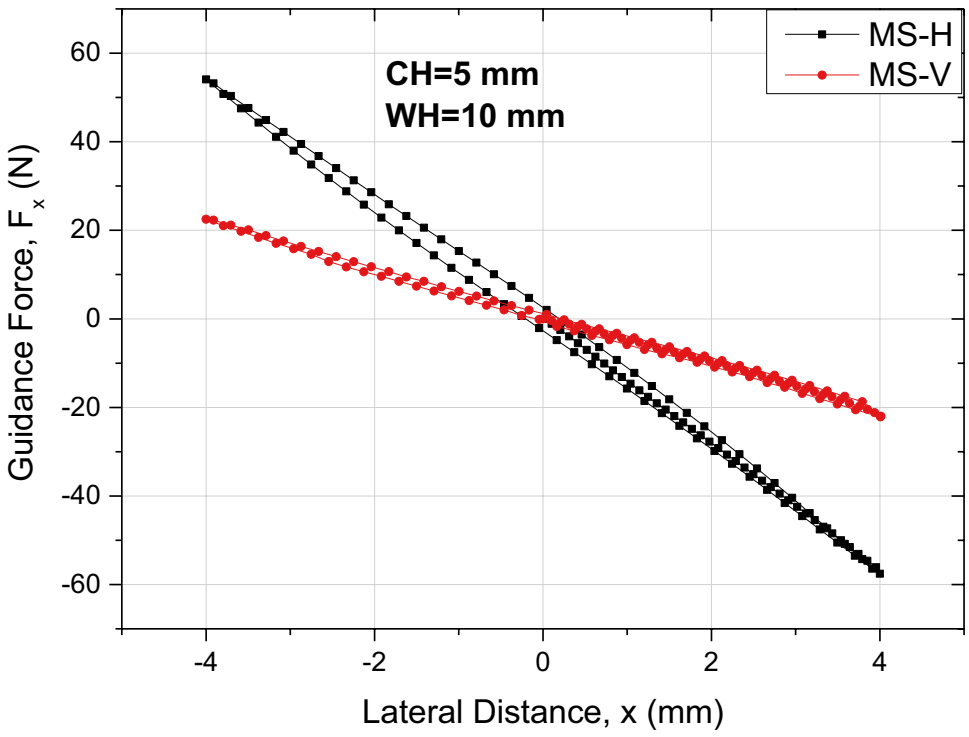


Fig. 4 Lateral guidance force comparison of multi-surface MS-H and MS-V arrangements in CH = 5 mm and WH = 10 mm

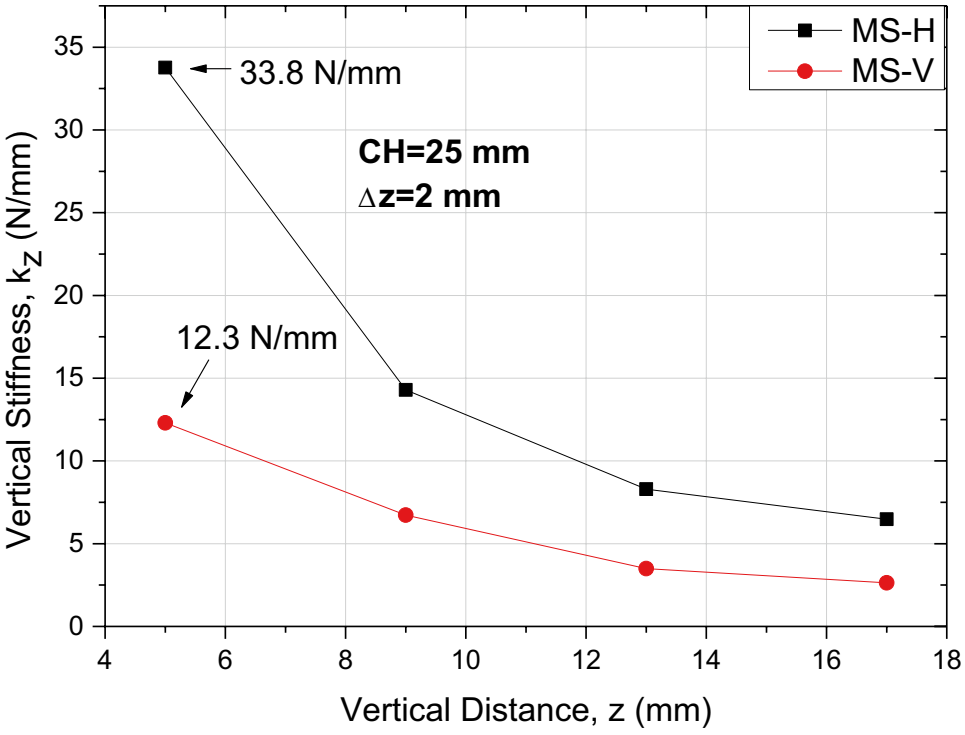


Fig. 5 Vertical magnetic stiffness comparison of multi-surface MS-H and MS-V arrangements in CH = 25 mm

in different CHs. After an impulse was applied in vertical direction, the free cryostats oscillate in the vertical directions as described by the following equations:

$$m\ddot{z} + c_z\dot{z} + k_{zD}z = 0, \tag{3}$$

where z, c_z, and k_{zD} represent the displacement of the levitated cryostat, damping coefficient, and dynamic stiffness, respectively, while m represents the total mass of the HTS chambers including HTSs. The dynamic stiffness in vertical direction is calculated as follows:

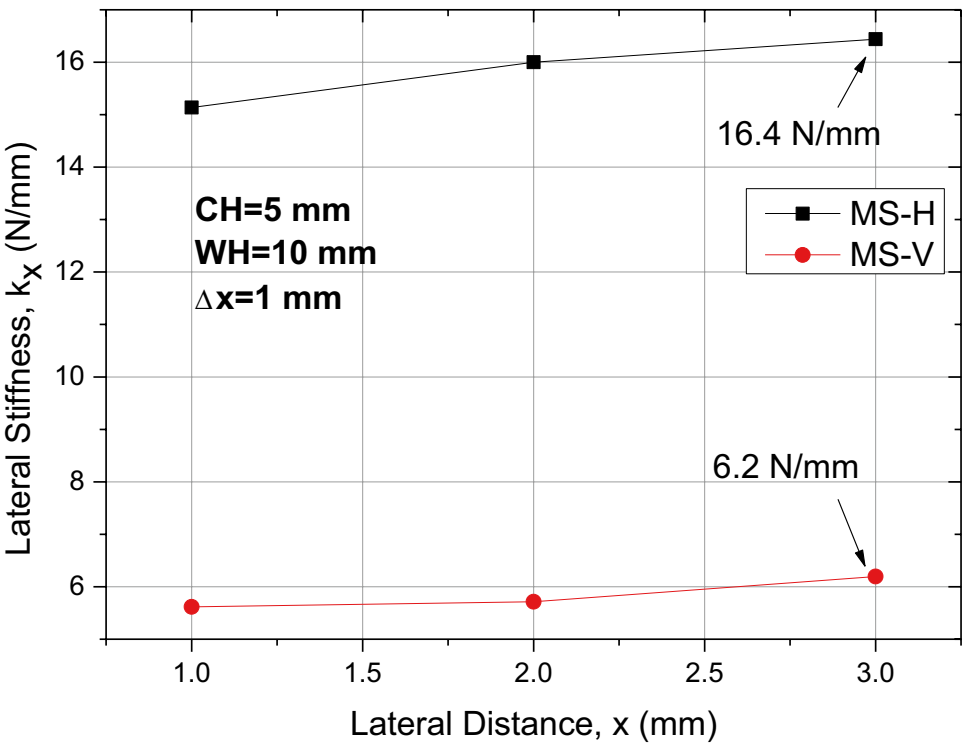


Fig. 6 Lateral magnetic stiffness comparison of multi-surface MS-H and MS-V arrangements in CH = 5 mm

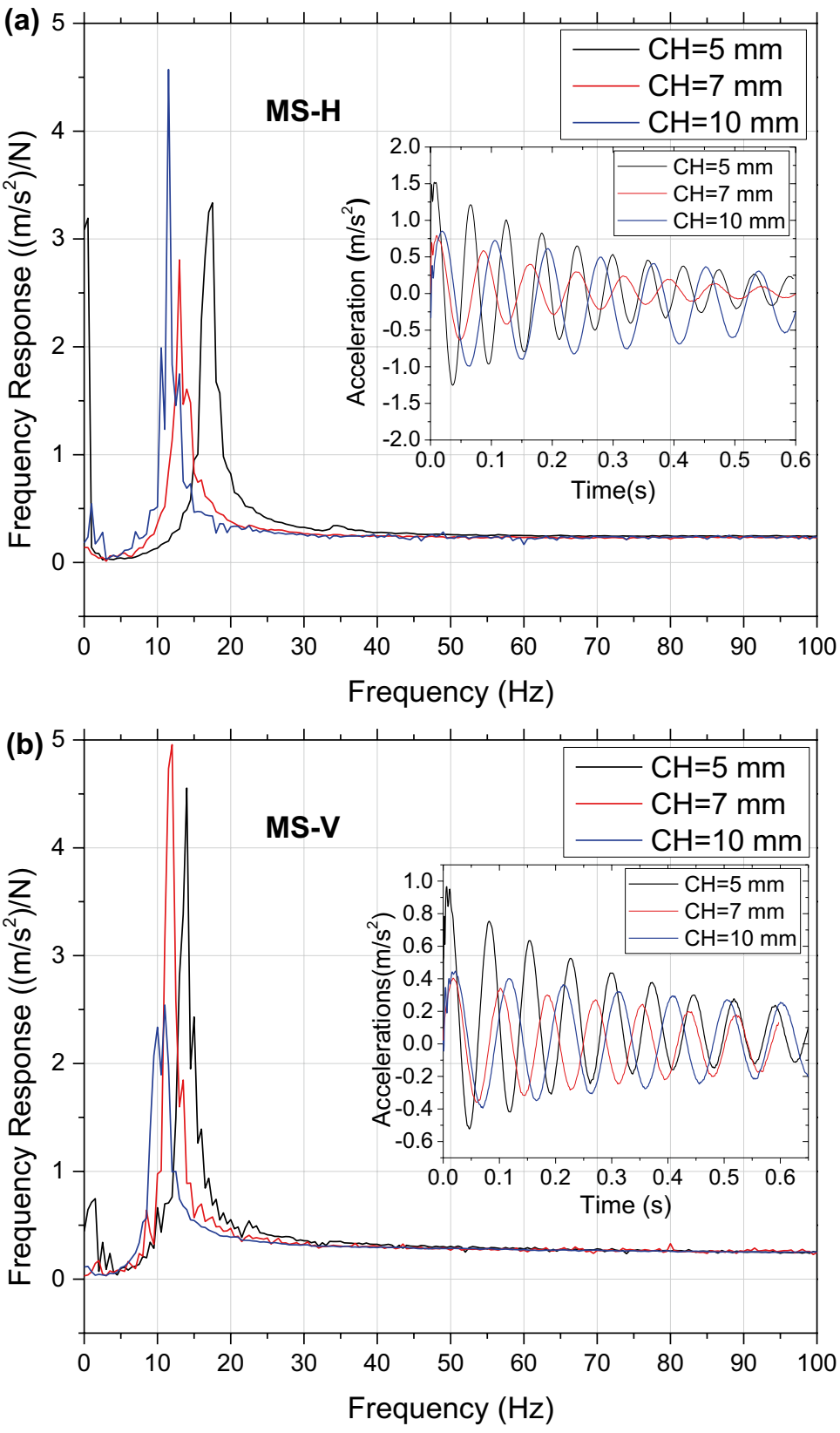


Fig. 7 Frequency-domain response of MS–H (**a**) and MS-V (**b**) arrangements in different CHs, after the pulse force was applied to the sample chamber by the hammer on the vertical direction. Insets show the related time-domain acceleration response graphs

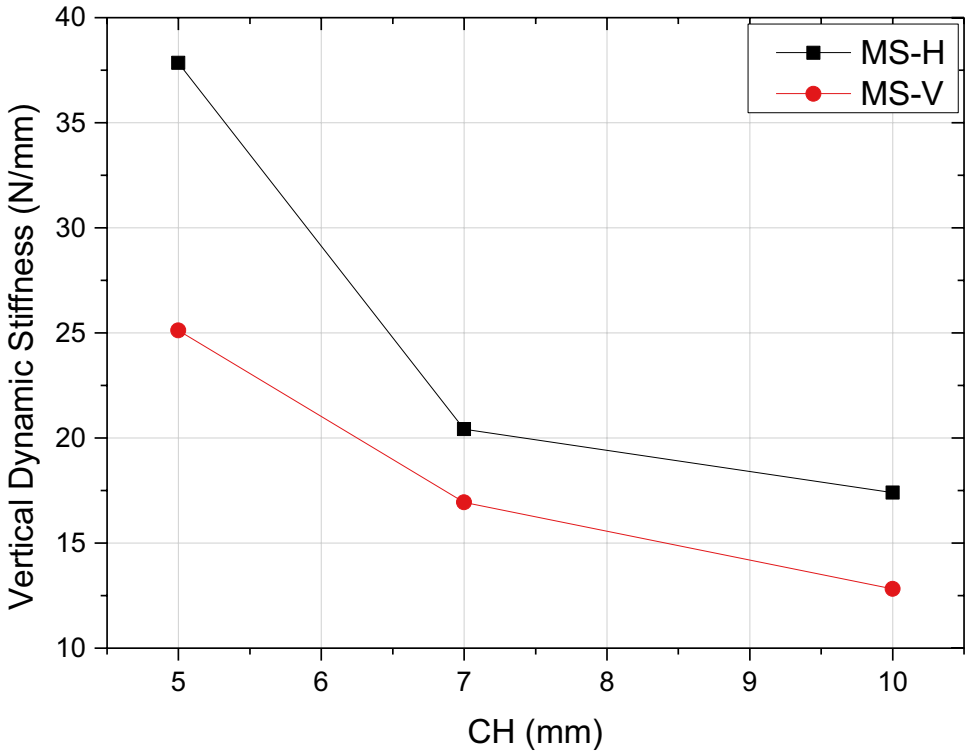


Fig. 8 Vertical dynamic stiffness comparison of MS-H and MS-V multi-surface HTS-PMG arrangements

$$w_n = \sqrt{k/m} \qquad k = m(2\pi f)^2 \tag{4}$$

where f represents the resonance frequency.

The frequency-domain response of MS-H arrangement is shown in Fig. 7 in different CHs, after the pulse force was applied by the hammer to top centre of the chambers. The insets of Fig. 7 show the related acceleration responses depending on time. The acceleration curves in the time domain have damping oscillation behaviour around the equilibrium point and decay rapidly with time. The frequency domain responses are obtained by applying FFT to the time domain responses in Fig. 7 inset. The vertical resonance frequencies of MS-H arrangement were determined from frequency response curves as 17.7 Hz, 13.0 Hz, and 12.0 Hz, respectively, in CH = 5 mm, 7 mm, and 10 mm. The same procedure was applied for MS-V arrangement, and the vertical resonance frequencies were respectively obtained as 14.0 Hz, 11.5 Hz, and 10 Hz. The vertical dynamic stiffness values of MS-H and MS-V arrangements, calculated from Eq. (3), are given in Fig. 8. The maximum dynamic stiffness values were obtained in CH = 5 mm as 37.8 N/mm and 25.1 N/mm for MS-H and MS-V arrangements, respectively. It is seen from this figure that the dynamic stiffness values increase with decreasing CH due to larger electromagnetic interaction density between the HTS and PMG in smaller vertical gaps. One can also see that the vertical dynamic stiffness values of MS-H arrangement are bigger than that of MS-V arrangement in all CHs. The bigger static and dynamic magnetic stiffness values of MS-H arrangement than that of MS-V arrangement indicate that the horizontal HTS-PMG geometry is more suitable for practical Maglev applications. On the other hand, it is seen by comparing Figs. 5 and 8 that the dynamic stiffness values of MS-V arrangement are bigger than that of static stiffness values. The physical base of bigger dynamic stiffness values of MS-V arrangement than static stiffness can be attributed to much more HTS/PMG ratio (and so magnetic interaction density) in MS-V arrangement (3/2) than that in MS-H arrangement (4/4 = 1). The magnetic stiffness can be likened to mechanical stiffness conceptually. When each HTS and PMG are considered as bonded points by mechanical spring due to the magnetic interaction, the interaction density in the vertical arrangement (similar to number of bonded points in mechanical spring) is bigger than the horizontal arrangement in small distances between the HTS and PMG units. This situation causes an increment in dynamic stiffness of MS-V arrangement in smaller CHs. Although more increment in dynamic stiffness of MS-V arrangement as compared to static stiffness is seen as a discrepancy, actually it indicates the different behaviour of vertical geometry as compared to horizontal geometry in small distances.

4 Conclusions

In this study, firstly, the magnetic flux density distributions of the horizontal and vertical PMGs were determined via numerical method using magnetostatic solution in COMSOL Multiphysics 3.5. Then, a detailed static and dynamic

experimental studies were performed in different CHs by using two different multi-surface HTS-PMG arrangements with horizontal and vertical geometries to determine the optimum magnetic force, static stiffness, dynamic response, and dynamic stiffness parameters of superconducting Maglev system. The maximum levitation force values are obtained as 202 N and 84 N, respectively, for MS-H and MS-V arrangements, while the maximum guidance force values are obtained as −58 N and −22 N. Nearly three times bigger maximum guidance force value of MS-H arrangement than that of MS-V can be attributed to bigger B_z value of MS-H arrangement. The difference between the maximum values in guidance force of MS-H and MS-V arrangements is obtained bigger than that in levitation force values indicating that the contribution of horizontal geometry to the guidance force is bigger than that of vertical geometry. The obtained bigger maximum vertical stiffness value of MS-H arrangement as 33.8 N/mm than that of MS-V arrangement as 12.3 N/mm indicates that the MS-H arrangement is more suitable for higher loadings and more resistant to external disturbances. As a conclusion, it can be said that the bigger levitation force, guidance force, and both static and dynamic magnetic stiffness values of MS-H arrangement with horizontal geometry than that of MS-V arrangement with vertical geometry indicate that the horizontal HTS-PMG geometry is more suitable for practical Maglev applications in terms of loading capacity and movement stability.

Acknowledgements This work was supported by the Scientific and Technological Research Council of Turkey (TUBITAK–Turkey), with project number 118F426.

References

1. Ainslie, M.D., Fujishiro, H.: Modelling of bulk superconductor magnetization. Supercond. Sci. Technol. **28**(5), 53002 (2015). https://doi.org/10.1088/0953-2048/28/5/053002
2. Bhagurkar, A.G., et al.: High trapped fields in C-doped MgB2 bulk superconductors fabricated by infiltration and growth process. Sci. Rep. **8**(1), 13320 (2018). https://doi.org/10.1038/s41598-018-31416-3
3. Savaskan, B., Guner, S.B., Yamamoto, A., Ozturk, K.: Trapped magnetic field and levitation force properties of multi-seeded YBCO superconductors with different seed distance. J. Alloy. Compd. **829**, 154400 (2020). https://doi.org/10.1016/j.jallcom.2020.154400
4. Guner, S.B., Abdioglu, M., Ozturk, K., Celik, S.: The comparison of levitation and lateral force of bulk and cut-pasted bulk GdBCO samples at different temperatures. J. Alloy. Compd. **822**, 153637 (2020). https://doi.org/10.1016/j.jallcom.2019.153637
5. Jiang, D.H., Ma, G.T., Lin, Q.X., Xu, Y.Y., Wang, S.Y., Wang, J.S.: Levitation-Force investigation of high-temperature superconducting maglev system under different variations of the vertical displacement. J Supercond Nov Magn **25**(1), 25–30 (2012). https://doi.org/10.1007/s10948-011-1202-9
6. Sivrioglu, S., Basaran, S., Yildiz, A.S.: Multisurface HTS-PM levitation for a flywheel system. IEEE Trans. Appl. Supercond. **26**(8), 1–6 (2016). https://doi.org/10.1109/TASC.2016.2615076
7. Storey, J.G., Szmigiel, M., Robinson, F., Wimbush, S.C., Badcock, R.A.: Stiffness enhancement of a superconducting magnetic bearing using shaped YBCO bulks. IEEE Trans. Appl. Supercond. **30**(4), 1–6 (2020). https://doi.org/10.1109/TASC.2020.2982884
8. Jeong, J.-S., An, D., Hong, J.-P., Kim, H.-J., Jo, Y.-S.: Design of a 10-MW-class HTS homopolar generator for wind turbines. IEEE Trans. Appl. Supercond. **27**(4), 1–4 (2017). https://doi.org/10.1109/TASC.2017.2669140
9. Li, H., Deng, Z., Ke, Z., Yu, J., Ma, S., Zheng, J.: Curve negotiation performance of high-temperature superconducting maglev based on guidance force experiments and dynamic simulations. IEEE Trans. Appl. Supercond. **30**(1), 1–11 (2020). https://doi.org/10.1109/TASC.2019.2932283
10. Schultz, L., et al.: Superconductively levitated transport system—the SupraTrans project. IEEE Trans. Appl. Supercond. **15**(2), 2301–2305 (2005). https://doi.org/10.1109/TASC.2005.849636
11. Sotelo, G.G., de Oliveira, R.A.H., Costa, F.S., Dias, D.H.N., de Andrade, R., Stephan, R.M.: A full scale superconducting magnetic levitation (MagLev) vehicle operational line. IEEE Trans. Appl. Supercond. **25**(3), 1–5 (2015). https://doi.org/10.1109/TASC.2014.2371432
12. Kusada, S., et al.: The project overview of the HTS magnet for superconducting Maglev. IEEE Trans. Appl. Supercond. **17**(2), 2111–2116 (2007). https://doi.org/10.1109/TASC.2007.899691
13. Werfel, F.N., et al.: Large-scale HTS bulks for magnetic application. Physica C **484**, 6–11 (2013). https://doi.org/10.1016/j.physc.2012.03.007
14. Wang, J., et al.: The first man-loading high temperature superconducting Maglev test vehicle in the world. Physica C **378–381**, 809–814 (2002). https://doi.org/10.1016/S0921-4534(02)01548-4
15. Mattos, L.S., Rodriguez, E., Costa, F., Sotelo, G.G., de Andrade, R., Stephan, R.M.: MagLev-cobra operational tests. IEEE Trans. Appl. Supercond. **26**(3), 1–4 (2016). https://doi.org/10.1109/TASC.2016.2524473
16. Ozturk, K., Abdioglu, M., Karaahmet, Z.: Magnetic force and stiffness performances of Maglev system based on multi–surface arrangements with three-seeded bulk YBaCuO superconductors. Physica C. **578**, (2020). https://doi.org/10.1016/j.physc.2020.1353739
17. Badía-Majós, A., Aliaga, A., Letosa-Fleta, J., Alfonso, M.M., Roche, J.P.: Tradeoff modeling of superconducting levitation machines: theory and experiment. IEEE Trans. Appl. Supercond. **25**, 2015. https://doi.org/10.1109/TASC.2015.2448456
18. Liu, K., et al.: Experiment and simulation of superconducting magnetic levitation with REBCO coated conductor stacks. Supercond. Sci. Technol. **31**, (2018). https://doi.org/10.1088/1361-6668/aa987b
19. Sun, S., Deng, Z., Wang, G., Wan, L. and Zheng, J.: Levitation performance of an onboard high-temperature superconducting bulk unit with cryocooler direct cooling. Supercond. Sci. Technol. **33**, (2020). https://doi.org/10.1088/1361-6668/aba483
20. Yildizer, I., Cansiz, A., Ozturk, K.: Optimization of levitation and guidance forces in a superconducting Maglev system. Cryogenics **78**, 57–65 (2016). https://doi.org/10.1016/j.cryogenics.2016.06.007
21. Ozturk, K., Guner, S.B., Abdioglu, M., Demirci, M., Celik, S., Cansiz, A.: An analysis on the relation between the seed distance and vertical levitation force for the multi-seeded YBCO using the modified advanced frozen image (MAFI) and experimental methods. J. Alloy. Compd. **805**, 1208–1216 (2019). https://doi.org/10.1016/j.jallcom.2019.07.205

22. Abdioglu, M., Kabaer, M., Ozturk, K., Erdem, O., Celik, S.: Lateral position effect of auxiliary permanent magnets on the magnetic force properties of cylindrical YBCO. J Supercond Nov Magn **30**(10), 2933–2938 (2017). https://doi.org/10.1007/s10948-016-3685-x
23. Ozturk, K., Kabaer, M., Abdioglu, M., Patel, A., Cansiz, A.: Clarification of magnetic levitation force and stability property of multi-seeded YBCO in point of supercurrent coupling effect. J. Alloy. Compd. **689**, 1076–1082 (2016). https://doi.org/10.1016/j.jallcom.2016.08.069
24. Abdioglu, M., Ozturk, K., Gedikli, H., Ekici, M., Cansiz, A.: Levitation and guidance force efficiencies of bulk YBCO for different permanent magnetic guideways. J. Alloy. Compd. **630**, 260–265 (2015). https://doi.org/10.1016/j.jallcom.2015.01.044
25. Ozturk, K., Abdioglu, M., Sahin, E., Celik, S., Gedikli, H., Savaskan, B.: The effect of magnetic field distribution and pole array on the vertical levitation force properties of HTS Maglev systems of HTS Maglev systems. IEEE Trans. Appl. Supercond. **25**(4), (2015). https://doi.org/10.1109/TASC.2015.2417679
26. Del-Valle, N., Sanchez, A., Navau, C. and Chen, D.X.: A theoretical study of the influence of superconductor and magnet dimensions on the levitation force and stability of maglev systems. Supercond. Sci. Technol. **21**, (2008). https://doi.org/10.1088/0953-2048/21/12/125008
27. Xu, K.X., Wu, D.J., Jiao, Y.L., Zheng, M.H.: A fully superconducting bearing system for flywheel applications. Supercond. Sci. Technol. **29**, (2016). https://doi.org/10.1088/0953-2048/29/6/064001
28. Ozturk, K., et al.: Comparative study of the magnetic stiffness, levitation and guidance force properties of single and multi seeded YBCOs for different HTS-PMG arrangements. J. Alloy. Compd. **643**, 201–206 (2015). https://doi.org/10.1016/j.jallcom.2015.04.142
29. Basaran, S., Sivrioglu, S.: Radial stiffness improvement of a flywheel system using multi-surface superconducting levitation. Supercond. Sci. Technol. **30**(3), 35008 (2017). https://doi.org/10.1088/1361-6668/30/3/035008

Publisher's Note Springer Nature remains neutral with regard to jurisdictional claims in published maps and institutional affiliations.